Effect of Surface Structure on Shape Transformations of Gold Nanorods

Yanting Wang[†], S. Teitel[‡], and Christoph Dellago[§*]
Center for Biophysical Modeling and Simulation and Department of Chemistry, University of Utah, 315 South 1400 East Room 2020, Salt Lake City, Utah 84112-0850, and Department of Physics and Astronomy, University of Rochester, Rochester, New York 14627, and Faculty of Physics, University of Vienna, Boltzmanngasse 5, 1090 Vienna, Austria
(Dated: May 15, 2006)

Upon heating, elongated gold nanocrystals (nanorods) transform to a shorter and bulkier shape well below melting. Using molecular dynamics simulations, we have studied this process for three different nanorods consisting of about 3000 atoms; the rods have similar shape but different exposed surface facets. Our results show that the shape transformation strongly depends on the particular surface facets covering the nanorods. While nanorods with {111} surfaces maintain their shape and structure up to the melting temperature, those covered with {110} or {100} facets undergo a transformation during which a change in aspect ratio is accompanied by a reorientation of the interior face-centered-cubic lattice. This reorientation leads to a crystal mainly covered with highly stable {111} facets. While the transitions of the rods with {110} and {100} surfaces occur through essentially the same sliding plane mechanism, they are initiated at the surface and at an edge, respectively.

I. INTRODUCTION

The shape and interior structure of nanoscale materials are intimately linked due to their large surface-to-volume ratio. In view of the envisaged technological applications of such materials it is of great importance to understand the effect that shape and surface structure can have on the mechanical and thermodynamical properties of nanoparticles. It has been shown recently in experiments[1–4] and simulations[5–8] that in gold nanoparticles the competition between surface and bulk free energetics can drive shape changes and stabilize particular structures. Since surface processes such as roughening and surface melting strongly influence the surface free energetics, they most likely play an important role in the stability of nano-sized gold clusters.

Bulk metal surfaces can undergo numerous reorganization processes, such as surface relaxation, reconstruction, deconstruction, pre-roughening, roughening, disordering, and melting with increasing temperature[9]. Experiments performed by Hoss *et al.*[10] indicate that the gold {110} surface roughens at 680 K, and melts at 770 K, below the bulk melting temperature of $T_m = 1337$ K[11]. Molecular dynamics simulations of this surface carried out by Ercolessi *et al.*[12] with the "glue" model[13] found that a liquid-like surface disorder appears near $T \approx 1000$ K, below the melting temperature $T_m = 1357$ K of the glue model. In both experiment and simulation the thickness of the liquid film grows with temperature and diverges at the bulk melting temperature. X-Ray experiments[11,17] reveal that the gold {100} surface exhibits a thin, disordered surface film at $T > 1170$ K. The thickness of the liquid film, however, does not grow with temperature. Similar conclusions were found in simulations by Bilalbegović and Tosatti[18]. In contrast, molecular dynamics simulations by Carnevali *et al.*[14] of the well-packed gold {111} surface found that it remains stable up to the bulk melting temperature T_m. This finding is supported by experiments[15,16] that indicate that the gold {111} surface does not melt up to at least 1250 K.

Recent computer simulations[5,6] indicate that surface instabilities may also play a central role in the transformation of gold nanorods from a long to a shorter and wider shape that has been observed in laser heating experiments[2,3]. In the simulations, this shape change is accompanied by a bulk reorganization of the nanorod in which the interior fcc-lattice reorients so as to align with newly formed stable {111} surface facets. The shape and structural change is initiated at the {110} surface facets and is possibly related to the roughening transition of these facets. In particular, roughening of the {110} facets may lower, or even remove, the activation barrier opposing the transformation to the lower free energy shape. Similar reconstructions in gold nanorods with different size and geometry were also observed in the simulations of Diao, Gall and Dunn[7,8], who attribute the transition to tensile surface stresses.

In this paper we report on molecular dynamics simulations that we have carried out to clarify the role played by surface structure in the shape transformation. For

[†]University of Utah
[‡]University of Rochester
[§]University of Vienna
*Author to whom correspondence should be addressed. E-mail: Christoph.Dellago@univie.ac.at.

this purpose, we consider initial gold nanorods with their long sides covered primarily by one kind of low-index facet, namely, gold {111}, {110}, or {100}. These simulations confirm that gold nanorods covered with {111} facets remain stable until melting, while nanorods initially covered with other surface facets undergo a shape and structure transformation possibly related to instabilities of their facets or the edges. Some preliminary results of this study have already been included in Ref. 6.

The remainder of the paper is organized as follows. In Sec. II we describe the model and the algorithm used to identify surface and bulk atoms with different local structure. The initial structures of the three different nanorods are specified in Sec. III. In Sec. IV we present the results of continuous heating simulations and in Sec. V those of quasi-equilibrium heating simulations, in which the system is heated at a gentler rate. A discussion of the results and some conclusions are provided in Sec. VI.

II. MODEL AND METHODS

All our simulations were carried out with the so-called many-body "glue" potential that yields a satisfactory description of the bulk, defect and surface properties of gold[13]. In the "glue" model, the potential energy of a system of N atoms consists of a sum of pair potentials and a many-body "glue" energy:

$$V = \frac{1}{2}\sum_i \sum_{j\neq i} \phi\left(r_{ij}\right) + \sum_i U\left(n_i\right). \tag{1}$$

Here the sums run over all particles, $r_{ij} = |\mathbf{r}_i - \mathbf{r}_j|$ is the interatomic distance between atoms i and j, and $\phi(r)$ is the pair interaction energy. The many-body "glue" energy $\sum U(n_i)$ depends on the coordination numbers n_i defined for all atoms,

$$n_i = \sum_j \rho\left(r_{ij}\right), \tag{2}$$

where $\rho(r)$ is a short-ranged monotonically decreasing function of the interatomic distance r. Cutoffs of 3.9 Å for $\rho(r)$ and 3.7 Å for $\phi(r)$ are used and the equations of motion are integrated with the velocity Verlet algorithm[19] with a time step of 4.3 fs. A cell index method[19] is used to reduce the computational time from order N^2 to order N.

To identify surface atoms and distinguish them from atoms in the interior of the nanorod we have developed the so-called *cone algorithm*[20] . For a given particle, an associated *cone region* is defined as the region inside a cone with a certain side length a and a certain span angle θ, whose vertex resides on the particle. A *hollow cone* is a cone region with no other particles inside. A particle is considered to be on the surface if at least one associated hollow cone can be found for this particle. The parameters $a = 5$ Å and $\theta = \pi/3$ permit a robust identification of the surface atoms.

At high temperatures the shape of nano-sized clusters fluctuates strongly and it is useful to consider the average cluster shape. For a rod shaped cluster we consider the average cross-sectional shape perpendicular to the long axis (the $\hat{z}$ axis) of the rod, determined as follows. For each instantaneous configuration, the end caps of the rod are discarded, and the remaining surface atoms are projected onto the x–y plane. Repeating this procedure for a sequence of configurations throughout the simulation run, we use the center of mass of all these projected atoms to define the origin, and then divide the x–y plane into 100 even polar angles. The average position of the atoms within each angular division is computed, and this then defines the radial distance to the surface within each angular division.

During the heating process the shape change of the gold nanorods was monitored by calculating the radius of gyration

$$R_g(t) = \sqrt{\frac{1}{N}\sum_i [\mathbf{r}_i(t) - \mathbf{r}_c]^2}, \tag{3}$$

where the sum runs over all particles and $\mathbf{r}_c$ is the center of mass of the rod. The radius of gyration is large for rods with large aspect ratio and reaches its minimum value for a spherical shape.

The time evolution of the nanorod structure was followed by calculating bond order parameters[21]. The general idea of bond order parameters is to capture the symmetry of bond orientations regardless of the bond lengths. Bonds are defined as the vectors joining a pair of neighboring atoms with an interatomic distance of less than a certain cutoff radius (3.7 Å in our case). The local order parameters associated with a bond $\mathbf{r}$ are a set of numbers

$$Q_{lm}(\mathbf{r}) \equiv Y_{lm}(\theta(\mathbf{r}), \phi(\mathbf{r})), \tag{4}$$

where $\theta(\mathbf{r})$ and $\phi(\mathbf{r})$ are the polar and azimuthal angles of the bond with respect to an arbitrary fixed reference frame and $Y_{lm}(\theta(\mathbf{r}), \phi(\mathbf{r}))$ are the spherical harmonics. Only even-l spherical harmonics are considered so that they are invariant under inversion. Global bond order parameters can then be calculated by averaging $Q_{lm}(\mathbf{r})$ over all bonds:

$$\overline{Q}_{lm} \equiv \frac{1}{N_b}\sum_{\text{bonds}} Q_{lm}(\mathbf{r}), \tag{5}$$

where N_b is the number of bonds. To make the order parameters invariant with respect to rotations of the reference frame, the second-order invariants are defined as

$$Q_l \equiv \sqrt{\frac{4\pi}{2l+1}\sum_{m=-l}^{l} \left|\overline{Q}_{lm}\right|^2}, \tag{6}$$

and the third-order invariants are defined as

$$W_l \equiv \sum_{\substack{m_1, m_2, m_3 \\ m_1+m_2+m_3=0}} \begin{pmatrix} l & l & l \\ m_1 & m_2 & m_3 \end{pmatrix} \cdot \overline{Q}_{lm_1}\overline{Q}_{lm_2}\overline{Q}_{lm_3}, \tag{7}$$

TABLE I: Bond order parameters for 3D face-centered-cubic (fcc), hexagonal-close-packed (hcp), simple-cubic (sc), body-centered-cubic (bcc), liquid, and 2D gold {110} surface, gold {100} surface, and gold {111} surface structures.

Geometry	Q_4	Q_6	$\hat{W}_4$	$\hat{W}_6$
fcc	0.191	0.575	-0.159	-0.013
hcp	0.097	0.485	0.134	-0.012
sc	0.764	0.353	0.159	0.013
bcc	0.082	0.500	0.159	0.013
liquid	0	0	0	0
110 surface	1	1	0.134	-0.093
100 surface	0.829	0.586	0.125	-0.007
111 surface	0.375	0.741	0.134	-0.046

where the coefficients $(\cdots)$ are the Wigner $3j$ symbols[27]. *Reduced* order parameters, almost independent on the precise definition of nearest neighbors, can be defined as:

$$\hat{W}_l \equiv \frac{W_l}{\left(\sum_m |Q_{lm}|^2\right)^{3/2}}. \quad (8)$$

We used the four bond order parameters Q_4, Q_6, $\hat{W}_4$, and $\hat{W}_6$ to identify structures accurately. The values of these bond order parameters for perfect fcc, hcp, icosahedral, and liquid structures are listed in Table I.

Bond order parameters averaged over *all* bonds can be used to monitor *global* structural changes. We will also use the *local* bond order parameters, averaged over the bonds of each atom separately, to determine the local structure of each atom. For a surface atom, we average only over bonds to other surface atoms. In Table I we therefore also give the values of the bond order parameters for several perfect low-index planar facets.

Based on the local bond order parameter values, the following criteria are used to identify atoms with different local structures. For interior atoms: fcc if $Q_4 > 0.17$ and $\hat{W}_4 < -0.10$; hcp if $Q_4 < 0.13$ and $\hat{W}_4 > 0.07$. For surface atoms: on {111} facet if $0.7 < Q_6 < 0.9$ and $-0.08 < \hat{W}_6 < -0.02$; on {100} facet if $Q_6 < 0.7$ and $\hat{W}_6 > -0.02$; on {110} facet if $Q_6 > 0.9$ and $\hat{W}_6 < -0.08$. The atoms in the following figures will be colored accordingly. For interior atoms: golden atoms have a local fcc structure, green atoms have a local hcp structure, and gray atoms are neither. For surface atoms: golden atoms are {111} facets, green atoms are {100} facets, red atoms are {110} facets, and gray are others.

III. INITIAL CONFIGURATIONS

The initial configurations of the gold nanorods were carved out from an fcc-crystal in three different ways to obtain gold rods mostly covered by {111}, {110}, or {100} facets. These manually constructed rods then went through a constant temperature MD simulation at $T = 5$ K for 10^6 steps (4.3 ns) to relax the surface. The potential energy of the final configuration was then minimized using the conjugate gradient method[25] to quench local thermal fluctuations.

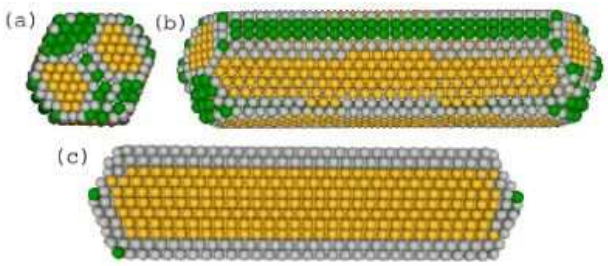

FIG. 1: Initial configuration of the {111} rod relaxed at 5 K. (a) View down the long axis; (b) Side view; (c) Cross-sectional view parallel to the long axis. In (a) and (b), golden atoms represent {111} facets, green atoms represent {100} facets, and gray atoms are on the edges. In (c), golden atoms have a local fcc structure, green atoms have a local hcp structure, and gray atoms have neither.

A. {111} Rod

The initial configuration for the gold nanrod mostly covered by {111} facets has its long axis along the ⟨110⟩ direction and has an aspect ratio of about 3. This rod has a cross-sectional area of about 2.8 nm × 2.8 nm and consists of 3411 atoms. The sides down the long axis of the rod consist mostly of {111} facets, with two narrow {100} facets added to truncate what would otherwise have been sharp edges where the {111} facets would meet at an acute angle; this truncation reduces the surface area and yields a more compact cross-sectional shape. The relaxed and minimized rod at 5 K, colored by its surface bond order parameters, is shown in Fig. 1. This rod will be referred to as the {111} rod.

B. {110} Rod

The second rod has its long axis in the ⟨100⟩ direction and is covered with {110} facets on the long sides and with {100} facets on the end caps. This rod has an aspect ratio of 3, a cross-sectional area of about 2.5 nm ×2.5 nm, and consists 2546 atoms. The relaxed and minimized configuration at $T = 5$ K is shown in Fig. 2. In this configuration the {110} surface facets are not readily identified by the local bond criteria given in Sec. II. This is due to the surface reconstruction[26], in which the atoms immediately underlying the initial {110} facet move upwards and become surface atoms. Nevertheless, the reconstructed {110} facets along the rod sides are still easily identified by direct visual inspection. This rod will be referred to as the {110} rod.

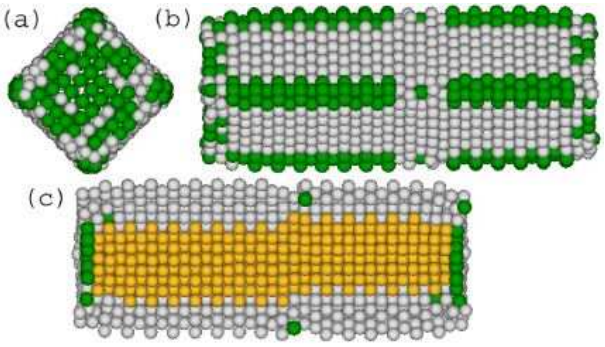

FIG. 2: Initial configuration of the {110} rod relaxed at 5 K. (a) View down the long axis; (b) Side view; (c) Cross-sectional view parallel to the long axis. In (a) and (b), green atoms represent {100} facets, and most gray atoms are actually on {110} facets. In (c), golden have a local fcc structure, green atoms have a local hcp structure, and gray atoms have neither.

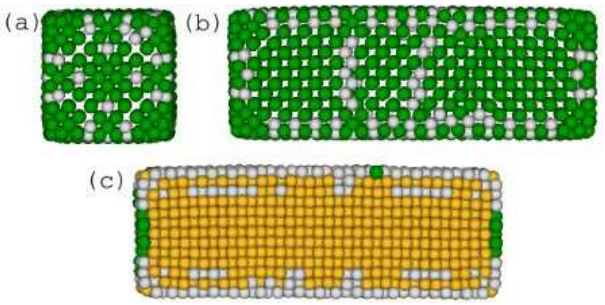

FIG. 3: Initial configuration of the {100} rod relaxed at 5 K. (a) View down the long axis; (b) Side view; (c) Cross-sectional view parallel to the long axis. In (a) and (b), green atoms represent {100} facets, and gray atoms are on the edges. In (c), golden atoms have a local fcc structure, green atoms have a local hcp structure, and gray atoms have neither.

C. {100} Rod

The third rod, carved out from the fcc-crystal with the long axis in ⟨100⟩ direction, is covered on all sides by six {100} facets. This rod has an aspect ratio of about 3, a cross-sectional area of about 2.44 nm ×2.44 nm, and consists of 3126 atoms. The relaxed and minimized configuration at $T = 5$ K is shown in Fig. 3. This rod will be referred to as the {100} rod.

IV. RESULTS FOR CONTINUOUS HEATING

To model the experimental procedure of laser heating used in the experiments of Link *et al.*[3], we heat the nanorods continuously from 5 K to complete melting at a rate of 7×10^{12}K/s, roughly in the range comparable to experiment[22]. The heating is done by rescaling the particle velocities after each molecular dynamics step such that the kinetic energy increases by a fixed amount. The whole heating procedure, in which the total energy of the cluster increases linearly in time, takes less than 10^5 simulation steps corresponding to about 430 ps.

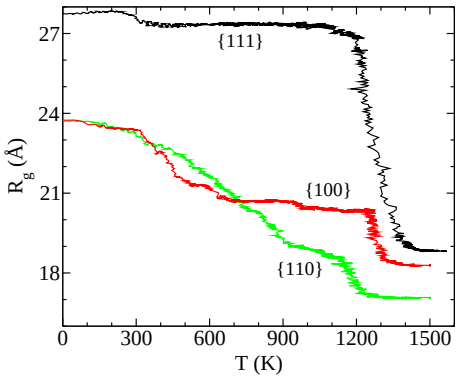

FIG. 4: Radius of gyration R_g as a function of instantaneous temperature T for the three different gold nanorods during the continuous heating procedure.

The shape changes of the gold nanrods were monitored by following the radius of gyration R_g as the cluster is heated (Fig. 4). Here, the instantaneous temperature is defined as $T = 2K/3N$, where K is the instantaneous total kinetic energy and N is the number of particles. Except for a small decrease near $T = 300$ K due to a reconstruction of the narrow {100} facets (green in Fig. 1) to a {111} structure, the {111} rod shows no noticeable shape change up to $T \simeq 1200$ K, when R_g rapidly decreases as the rod melts. In contrast, the shape of the {110} rod changes continuously from about 300 K to 900 K. A more gradual change then continues to about 1150 K, when the rod melts. Compared with the {110} rod, the {100} rod has a faster shape change from about 300 K to about 700 K, then its radius of gyration remains almost constant before the cluster melts at about 1250 K.

The time evolution of the global cluster structure during the heating procedure can be inferred from the average bond order parameters depicted in Fig. 5 as a function of temperature. Consistent with the shape stability of the {111} rod, its bond order parameters change only weakly up to the melting temperature. This remarkable stability of the {111} rod is due to the highly stable {111} facets covering most of the cluster surface. Of course, the elongated {111} rod is far from its true equilibrium shape that minimizes the total (bulk + surface) free energy; for the number of atoms considered here, our earlier simulations using the glue potential have found this equilibrium shape to be a Mackay icosahedron[20,23]. High free energy barriers related to the reorganization of bulk and surface, however, prevent the cluster from relaxing towards this true equilibrium shape within the time of the simulation (and of the typical experiment).

The behavior of the bond order parameters for the rods mainly covered with the less stable {110} and {100} facets is different. The bond order parameters for the {110} rod soften from about 300 K to about 700 K, corre-

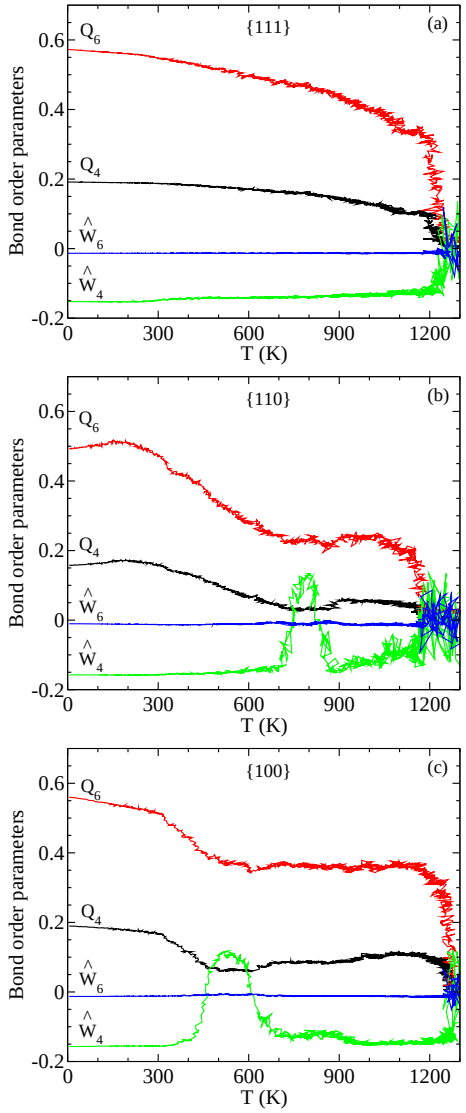

FIG. 5: Bond order parameters for (a) the {111} rod, (b) the {110} rod, and (c) the {100} rod during continuous heating.

sponding to its continuous shape change. Then, a structural change of the interior from fcc-dominated to hcp-like and then back to fcc occurs. This change is marked by a peak in $\hat{W}_4$ between 700 K and 900 K. For the {100} rod, a similar structural change takes place in the slightly lower temperature range from about 400 K to 700 K. Observation of the end product of this transformation above 900 K shows that this fcc-hcp-fcc process results in a complete reorientation of the original fcc-lattice axes, as the interior transforms to match newly forming stable {111} facets on the surface, thus lowering the total free energy of the cluster[6–8]. Considering the higher stability of the extended gold {100} surface with respect to the {110} surface it is interesting that the fcc-hcp-fcc transformation takes place at a lower temperature for the {100} rod than for the {110} rod. This unexpected behavior may be caused by a different temperature dependence of the

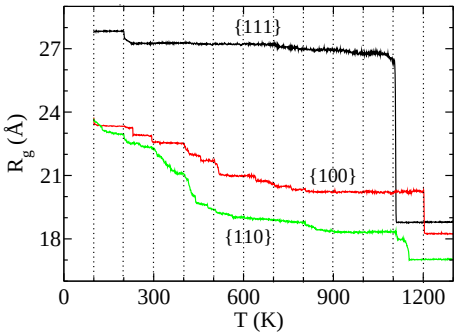

FIG. 6: Radius of gyration R_g as a function of temperature T for different gold nanorods during quasi-equilibrium heating.

free energy barriers opposing the transformation in the two cases. This would indicate that different mechanisms may be responsible for the transformation of the {110} and {100} rods. Below, we will show that, for slower heating, the onset for the structural transition of {110} rod shifts to lower temperatures while that of the {100} remains roughly the same.

V. RESULTS FOR QUASI-EQUILIBRIUM HEATING

In order to improve our understanding of the phenomena observed in the continuous heating simulations, we have carried out additional calculations with a much slower heating rate. In these *quasi-equilibrium* heating simulations the configurations relaxed at $T = 5$ K were first equilibrated at $T = 100$ K for 4.3 ns. Then, the temperature was incremented from $T = 100$ K to 1200 K in steps of 100 K. At each temperature the rod went through a molecular dynamics simulation of 4.3 ns duration. The effective heating rate is 2.3×10^{10} K/s, about 300 times slower than the continuous heating.

The shape changes of the gold nanrods were monitored by following the radius of gyration during the heating procedure (see Fig. 6). In the figure, the vertical dotted lines divide the temperature axis into equal sections. In each section, the radius of gyration is plotted as a function of increasing time for a constant temperature corresponding to the value at the left end point of the section.

As in the continuous heating case, the {111} rod does not show any pronounced shape change before melting at $T = 1100$ K, except for a small relaxation at $T = 200$ K related to the reconstruction of the narrow {100} facets. The {110} rod displays a marked shape change from 100 K to about 400 K, followed by a more gradual change up to 900 K. It then remains stable up to the melting temperature of 1100 K. In this intermediate state before melting the {110} rod has an aspect ratio of about 1.8. In contrast to the {110} rod, the {100} rod changes its shape in a more step-like manner from 200 K to 800 K. The

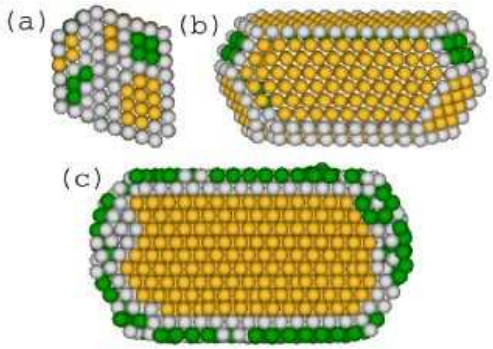

FIG. 7: Configuration of the {110} rod after quasi-equilibrium heating to 900 K.(a) View done the long axis; (b) Side View; (c) Cross-sectional view parallel to the long axis. In (a) and (b), golden atoms represent {111} facets, green atoms represent {100} facets, and gray atoms are on the edges. In (c), golden atoms have a local fcc structure, green atoms have a local hcp structure, and gray atoms have neither. For clarity, the surface layer and the first sub-surface layer have been removed in (a) and (b).

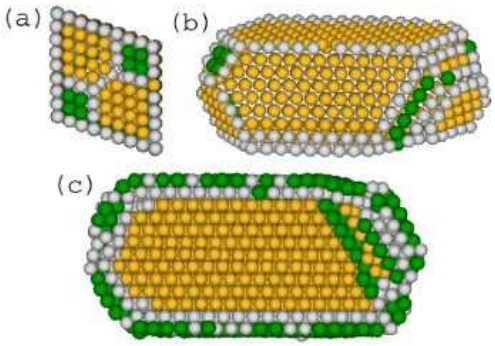

FIG. 8: Configuration of the {100} rod after quasi-equilibrium heating to 900 K. (a) View done the long axis; (b) Side View; (c) Cross-sectional view parallel to the long axis. In (a) and (b), golden atoms represent {111} facets, green atoms represent {100} facets, and gray atoms are on the edges. In (c), golden atoms have a local fcc structure, green atoms have a local hcp structure, and gray atoms have neither. For clarity, the surface layer and the first sub-surface layer have been removed in (a) and (b).

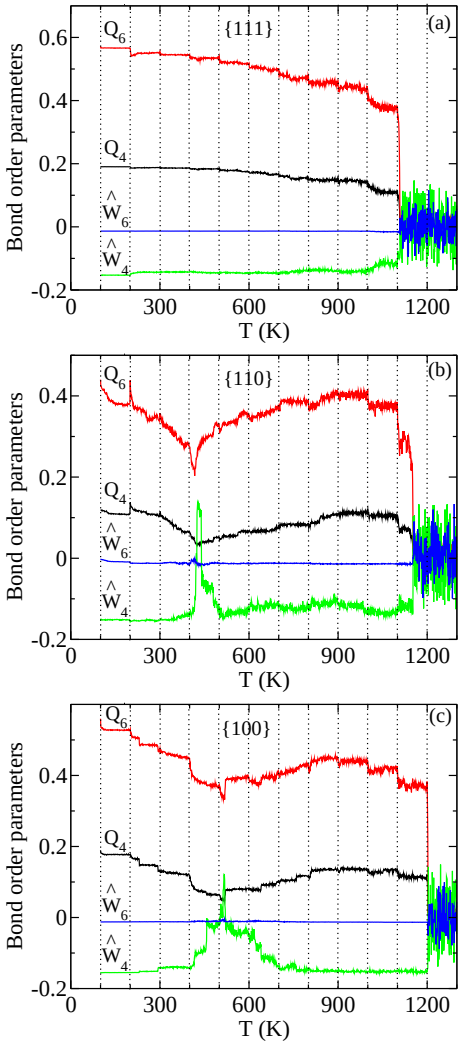

FIG. 9: Bond order parameters for (a) the {111} rod, (b) the {110} rod, and (c) the {100} rod, during quasi-equilibrium heating.

resulting intermediate state with an aspect ratio of about 1.9 is then stable up to its melting temperature of $T = 1200$ K. Both the high-temperature intermediate states of the {110} rod and the {100} rod have fcc-lattices that are reoriented with respect to their initial configuration and are covered with stable {111} facets (see Figs. 7 and 8).

Average bond order parameters that are a signature for the global structure of the clusters, are plotted in Fig. 9. Essentially, these curves show the same behavior observed in the continuous heating runs and shown in Fig. 5: the structure of the {111} rod changes only weakly up to melting and the fcc-hcp-fcc transition occurs for both the {110} and the {100} rods.

In contrast to the continuous heating procedure, however, the {110} rod undergoes the transition at a considerably lower temperature while the transition temperature for the {100} rod remains unchanged. This result is consistent with the lower stability of the {110} facets with respect to the {100} facets and indicates that the higher transition temperature for the {110} rod with faster heating is indeed a kinetic effect. Moreover, for the {100} rod the transition now occurs in a step-like manner over a wider range than in the continuous heating case. All this suggests that the transition may follow different mechanisms for the {110} rod and the {100} rod.

To obtain additional insight into the nature of the transition we computed the average cross-sectional shapes of the {110} rod and the {100} rod. These results are displayed in Fig. 10. For the {110} rod shown in Fig. 10(a), the average cross-sectional shape does not change significantly from 100 K to 200 K. From 300 K to 400 K, how-

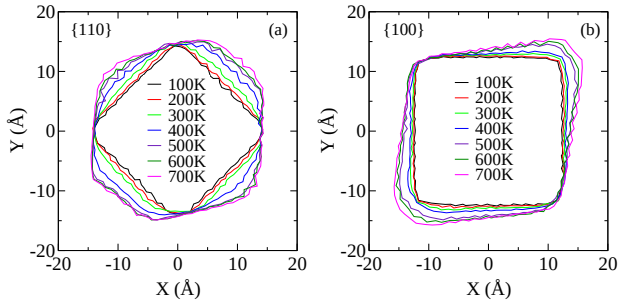

FIG. 10: Average cross-sectional shapes, viewed down the long axis of the rod, for (a) the {110} rod and (b) the {100} rod.

ever, the four {110} facets are rounded and bulge out. This temperature range coincides with the onset of the fcc-hcp-fcc transformation. From 500 K to 700 K, and at higher temperatures not shown, the sides of the rod relax and reorganize to form stable {111} facets. Interestingly, the four corners of the initial cross-sectional shape remain at fixed positions during the whole transformation. This indicates that for the {110} rod the surface edges do not play an important role during the shape change and that the process driving the transformation most likely involves the properties of the {110} facets.

In contrast to the {110} rod, the {100} rod, shown in Fig. 10(b), has a cross-sectional shape that changes mostly at the edges between the flat facets. Below $T = 500$ K, the average shape of the {100} rod only exhibits slight changes with some rounding of the corners. At $T = 500$ K the average cross-sectional shape rapidly changes from square to rhombic. During this shape change, that yields a rod predominantly covered with {111} facets, the top-left and the bottom-right corners remain at fixed positions while the two other corners bulge out. Throughout, the facets of the rod keep almost perfectly flat and do not disorder. Considering the importance of the free-energy contribution from vertices and edges in the stability of nanomaterials[20,23,24], it is conceivable that the transformation mechanism is related to a thermal instability of the edges.

The interior structure of the {110} and {111} rods as they are heated from 100 K is illustrated in Fig. 11. For these cross-sectional views thermal fluctuations were quenched by conjugate gradient minimization[25]. The atoms are colored according to their local structure as determined from the local bond order parameters.

The {110} rod, initially covered by an irregular surface, begins to bend at 200 K when an hcp region starts to form on the bottom side of the rod. This hcp region then propagates through the rod by a sliding of {111} planes leaving behind an fcc-region with changed orientation. The structural change in the interior is accompanied by the formation of {111} surface facets. At 700 K the transition is mostly completed and the rod has reached its high-temperature intermediate state (see Fig. 7). A similar mechanism was suggested in Link et al.[4]

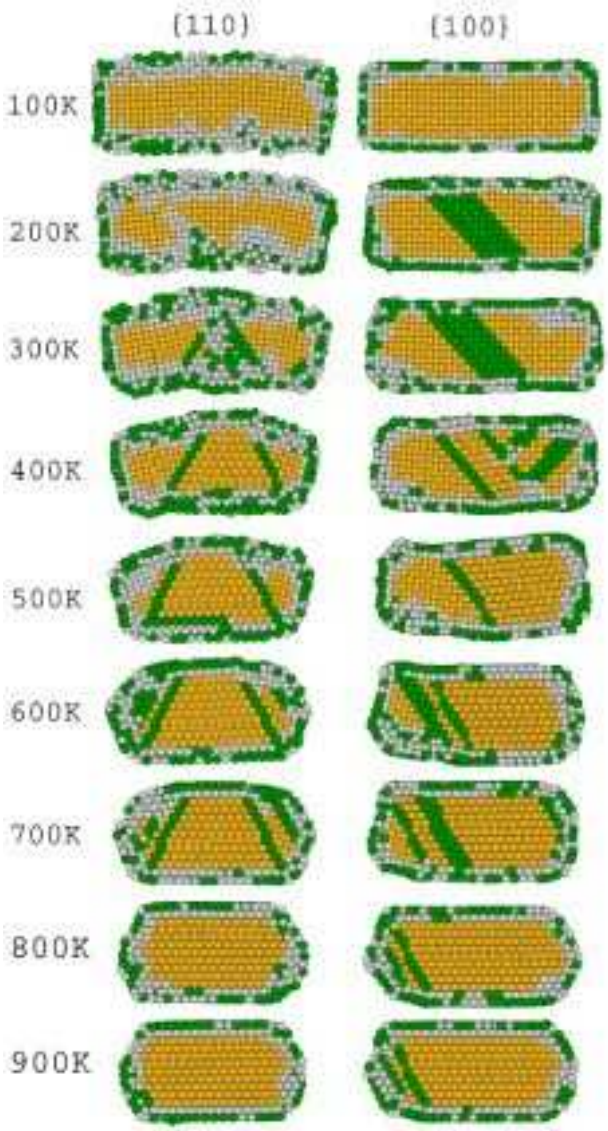

FIG. 11: Cross-sectional view for the {110} rod (left) and the {100} rod (right) at various temperatures. Atoms are colored according to local crystal structure: fcc is yellow, hcp is green, and neither is grey.

to explain their laser heating experiments, however they proposed that the instability nucleates in the interior and spreads outwards to the surface; our results suggest the reverse, with the instability being nucleated at the surface, and proceeding inwards

Unlike the {110} rod, the surface of the {100} rod remains mostly ordered throughout the heating procedure. The transition from fcc to hcp and back to fcc starts at 200 K when layers of atom slide with respect to each other near the rod center. This configuration remains almost unchanged at 300 K, in contrast to the pronounced change occurring in the {110} rod at this temperature. At the end of 400 K, the middle planes have returned to an fcc structure, but with a changed orientation of the

fcc lattice axes. As the hcp layers continue to propagate through the rod, more and more of the surface becomes covered with {111} facets. During the incomplete stages of the transformation the rod is slightly bent, but at 700 K the straight intermediate high-temperature structure is reached (see Fig. 8).

While the final state is very similar for both the {110} rod and the {100} rod, the relaxation mechanism by which it is achieved is rather different, as can be inferred from Figs. 9-11. For the {110} rod the fcc-hcp-fcc transformation seems to be favored by the roughened surface. The transformation in the {100} rod, on the other hand, does not appear to be related to a surface instability but rather originates at an edge.

VI. CONCLUSIONS AND DISCUSSION

We have performed molecular dynamics simulations of three different gold nanorods heated from a temperature of 5K to melting. The nanorods all consisted of about 3000 atoms and had an initial shape with an aspect ratio of 3 but were covered with different low-index surface facets. Our simulations reveal that the thermal stability of the rods strongly depends on the type of exposed surface facets. Rods mostly covered with {111} facets essentially maintain their initial elongated shape up to the melting temperature. Rods covered by {110} and {100} facets, on the other hand, undergo a transition to a shorter and bulkier shape well below melting. During this transition, sliding planes cause the interior structure of the rods to change from fcc to hcp and back to fcc. The new fcc lattice is reoriented with respect to the initial one, leading to a rod mostly covered with stable {111} facets.

While the interior transformations of the {110} and the {100} rod occur through essentially the same sliding plane mechanism, they appear to be initiated by different events. The results of our simulations indicate that for the transformation of the {100} rod the edges seem to play a central role. The transformation of the {110} rod, on the other hand, most likely nucleates at the surface facets. In this case, the activation barrier for the structural and shape transformation of the nanorod may be reduced by the roughening transition of this surface. Such roughening occurs at 680 K for macroscopic {110} gold surfaces. For finite size surfaces such as nanocluster facets, however, enhanced fluctuations are expected to lower the roughening temperature[28] such that it may indeed coincide with the onset of the transformation observed in our {110} rod.

The transformation mechanisms discussed above for gold nanorods may well exist in other simple elemental metals. For example, the silver {110} surface has a roughening transition temperature of 600 K and a melting temperature of 1235 K[29]. The lead {110} surface has a roughening temperature of 415 K and a melting temperature of 601 K[30]. However, further studies will be required to clarify the role played by surface and edge instabilities in the nucleation of structural and shape transformations in metal nanoclusters.

Acknowledgments

This work was supported by the Austrian Science Fund (FWF) under Grant No. P17178-N02.

[1] Y. Kondo and K. Takayanagi, *Phys. Rev. Lett.* **79**, 3455 (1997).

[2] Z. L. Wang, M. B. Mohamed, S. Link, and M. A. El-Sayed, *Surf. Sci.* **440**, L809 (1999).

[3] S. Link, C. Burda, B. Nikoobakht, and M. A. El-Sayed, *J. Phys. Chem. B* **104**, 6152 (2000).

[4] S. Link, Z. L. Wang, M. A. El-Sayed, *J. Phys. Chem B* **104**, 7867 (2000).

[5] Y. Wang and C. Dellago, *J. Phys. Chem. B* **107**, 9214 (2003).

[6] Y. Wang, S. Teitel, and C. Dellago, *Nano Lett.* **5**, 2174 (2005).

[7] J. Diao, K. Gall, and M. L. Dunn, *Nat. Mater.* **2**, 656 (2003).

[8] J. Diao, K. Gall, and M. L. Dunn, *Phys. Rev. B* **70**, 075413 (2004).

[9] F. D. Di Tolla, E. Tosatti, and F. Ercolessi, *Interplay of melting, wetting, overheating and faceting on metal surfaces: theory and simulation, in Monte Carlo and molecular dynamics of condensed matter systems*, K. Binder and G. Ciccotti (Eds.), Societá Italiana di Fisica, Bologna, p. 345-398 (1996).

[10] A. Hoss, M. Nold, P. von Blanckenhagen, and O. Meyer, *Phy. Rev. B* **45**, 8714 (1992).

[11] B. M. Ocko, D. Gibbs, K. G. Huang, D. M. Zehner, and S. G. J. Mochrie, *Phys. Rev. B* **44**, 6429 (1991).

[12] F. Ercolessi, S. Iarlori, O. Tomagnini, E. Tosatti, and X. J. Chen, *Surf. Sci.* **251/252**, 645 (1991).

[13] F. Ercolessi, M. Parrinello, and E. Tosatti, *Philos. Mag. A* **58**, 213 (1988).

[14] P. Carnevali, F. Ercolessi, and E. Tosatti, *Phys. Rev. B* **36**, 6701 (1987).

[15] K. G. Huang, D. Gibbs, D. M. Zehner, A. R. Sandy, and S. G. J. Mochrie, *Phys. Rev. Lett.* **65**, 3313 (1990).

[16] G. M. Watson, D. Gibbs, S. Song, A. R. Sandy, S. G. J. Mochrie, and D. M. Zehner, *Phys. Rev. B* **52**, 12329 (1995).

[17] S. G. J. Mochrie, D. M. Zehner, B. M. Ocko, and D. Gibbs, *Phys. Rev. Lett.* **64**, 2925 (1990).

[18] G. Bilalbegović and E. Tosatti, *Phys. Rev. B* **48**, 11240 (1993).

[19] M. P. Allen and D. J. Tildesley, *Computer Simulation of Liquids*, Clarendon Press: Oxford (1987).

[20] Y. Wang, S. Teitel, and C. Dellago, *J. Chem. Phys.* **122**, 214722 (2005).

[21] P. J. Steinhardt, D. R. Nelson, and M. Ronchetti, *Phys. Rev. B* **28**, 784 (1983).
[22] S. Link, C. Burda, B. Nikoobakht, and M. A. El-Sayed, *Chem. Phys. Lett.* **315**, 12 (1999).
[23] Y. Wang, S. Teitel, and C. Dellago, *Chem. Phys. Lett.* **394**, 257 (2004).
[24] Y. Zhao and B. I. Yakobson, *Phys. Rev. Lett.* **91**, 35501 (2003).
[25] W. H. Press, S. A. Teukolsky, W. T. Vetterling, and B. P. Flannery, *Numerical Recipes in C: The Art of Scientific Computing*, Cambridge University Press: Cambridge (1992).
[26] D. Wolf, H. Jagodzinski, and W. Moritz, *Surf. Sci.* **77**, 265 (1978).
[27] L. D. Landau and F. M. Lifshitz, *Quantum Mechanics*, Pergamon: New York (1965).
[28] J. Kohanoff, G. Jug, and E. Tosatti, *J. Phys. A* **23**, L209 (1990).
[29] L. Pedemonte and G. Bracco, *Surf. Sci.* **513**, 308 (2002).
[30] H.-N. Yang, T.-M. Lu, and G.-C. Wang, *Phys. Rev. Lett.* **63**, 1621 (1989).